

# Field-free Three-Dimensional Orientation of Asymmetric-Top Molecules

Kang Lin,<sup>1</sup> Ilia Tutunnikov,<sup>2</sup> Junjie Qiang,<sup>1</sup> Junyang Ma,<sup>1</sup> Qiying Song,<sup>1</sup> Qinying Ji,<sup>1</sup> Wenbin Zhang,<sup>1</sup> Hanxiao Li,<sup>1</sup> Fenghao Sun,<sup>1</sup> Xiaochun Gong,<sup>1</sup> Hui Li,<sup>1</sup> Peifen Lu,<sup>1</sup> Heping Zeng,<sup>1</sup> Yehiam Prior,<sup>2</sup> Ilya Sh. Averbukh,<sup>2</sup> and Jian Wu<sup>1,3</sup>

<sup>1</sup>State Key Laboratory of Precision Spectroscopy, East China Normal University, Shanghai 200062, China

<sup>2</sup>Department of Chemical and Biological Physics, Weizmann Institute of Science, Rehovot 7610001, Israel

<sup>3</sup>Collaborative Innovation Center of Extreme Optics, Shanxi University, Taiyuan, Shanxi 030006, China

Alignment and orientation of molecules by intense, ultrashort laser fields are crucial for a variety of applications in physics and chemistry. These include control of high harmonics generation<sup>1,2</sup>, molecular orbitals tomography<sup>2-4</sup>, control of molecular photoionization and dissociation processes<sup>5-7</sup>, production of “molecular movies” with the help of X-ray free-electron laser sources and ultrafast electron diffraction of relativistic electrons<sup>8-10</sup>. While the dynamics of laser-induced molecular alignment has been extensively studied and demonstrated (for a review, see<sup>11-14</sup>), molecular orientation is a much more challenging task, especially for asymmetric-top molecules. Here we report the first experimental demonstration of a field-free, all-optical three-dimensional orientation of asymmetric-top molecules by means of phase-locked cross-polarized two-color laser pulses. In addition to the conventional integrated orientation factor, we report the differential degree of orientation which is not amenable to optical measurements, but is readily accessible in our angle-resolved imaging technique. Our scheme applies to a wide class of asymmetric molecules and opens new ways towards controlling their orientation, eventually leading to direct imaging of structure of gas-phase molecules<sup>15</sup> using advanced free electron laser beams with extremely high spatiotemporal resolution.

Over the years, several approaches have been used to break the symmetry and define preferred directions in space so that molecules can be oriented. Early on, intense nonresonant laser fields were combined with weak electrostatic fields<sup>16-20</sup> for symmetry breaking, and this was followed by introduction of single-cycle THz pulses<sup>21-26</sup>, alone or in combination with optical pulses<sup>27-30</sup>. More recently, pulsed laser fields with twisted polarization were shown to be effective for orienting generic asymmetric molecules<sup>31</sup>, and for enantioselective orientation of chiral molecules<sup>32,33</sup>. Of special interest for us is an all-optical approach that uses nonresonant two-color laser field (fundamental wave and its second harmonic) where the orientation is achieved via the nonlinear interaction with the molecular hyperpolarizability<sup>22,34-40</sup>.

In the present work, we report the first experimental demonstration of all-optical field-free three-dimensional (3D) orientation of asymmetric-top molecules. We introduce a scheme using phase-locked Orthogonal Two-Color (OTC) laser fields, which is applicable to a large class of polyatomic molecules. In our experiments, the fundamental field aligns the major molecular axis (the one with the highest polarizability) along the polarization di-

rection. The second harmonic field is temporally overlapping with the fundamental field. The two fields together couple to the molecule via off-diagonal components of the molecular hyperpolarizability tensor. This interaction orients the minor molecular axis (the one with the second highest polarizability) after the OTC pulse is over and results in field-free, 3D molecular orientation. In what follows, we describe the experimental setup, show the results of experimental observations, provide a simplified two dimensional (2D) model that illustrates the principles of our method, and discuss the results of a more sophisticated fully three-dimensional simulation of the experimental measurements.

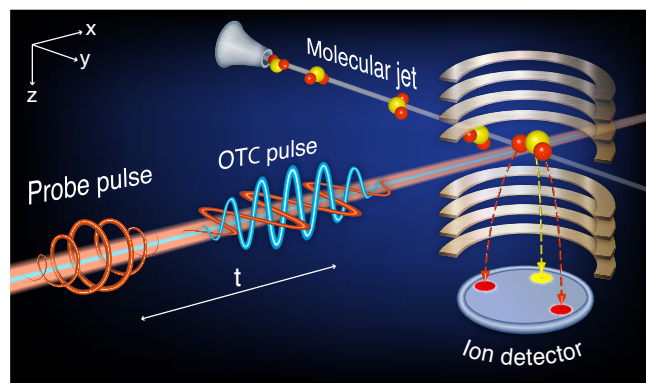


FIG. 1. **Layout of the experiment.** A supersonic gas jet of  $\text{SO}_2$  molecules subject to a pair of synchronized two-color laser pulses with orthogonal polarizations in an ultrahigh vacuum chamber of COLTRIMS.

The experiments were performed on Sulphur dioxide ( $\text{SO}_2$ ) molecules in a supersonic molecular beam (rotational temperature  $T = 18 \text{ K}$ ). The O-axis (see Fig. 2a) is the major molecular axis with the largest polarizability. The S-axis bisects the bond angle between the oxygen atoms, and it is the minor axis with the second highest polarizability. The molecular permanent dipole moment is directed along the S-axis. In our scheme, the laser pulses propagate along the X axis. The fundamental field is a Y-polarized femtosecond laser pulse with the fundamental wavelength (FW) of 790 nm. The second color field is a Z-polarized second harmonic (SH) pulse of 395 nm whose frequency is doubled relative to FW. It temporally and spatially overlaps the first pulse, and is phase locked to it. The OTC pulse is focused on a supersonic molecular beam propagating along the Y axis. At a variable delay after the application of the two-color pulse, an intense circularly polarized probe pulse is employed to explode the molecules and to image their 3D spatial orientation via coincident Coulomb explosion imaging technique, as is schematically shown in Fig. 1. The reaction microscope of Cold Target Recoil Ion Momentum Spec-

troscopy (COLTRIMS) setup<sup>41</sup> provides direct access to the spatiotemporal molecular dynamics as a function of the time delay after the OTC pulses with femtosecond time-resolution. The details of the experimental system are given in Methods Subsection A.

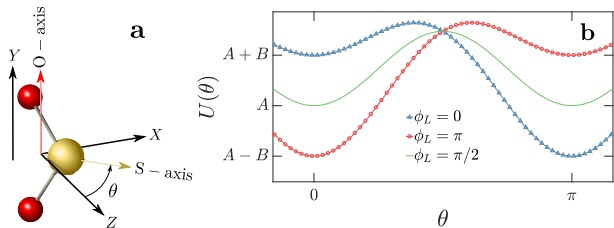


FIG. 2. **2D model.** **a**, SO<sub>2</sub> molecule whose major axis is perfectly aligned along the laboratory Y axis. The minor axis lies in the XZ plane at an angle  $\theta$  relative to the Z axis. **b**, Potential energy as a function of  $\theta$  for  $\phi_L = 0, \pi, \pi/2$ , (see eqs. 3 and 4)

To illustrate the two-color orientation mechanism, we consider a classical ensemble of cold SO<sub>2</sub> molecules whose major axis is perfectly aligned along the laboratory Y axis with a uniform angular distribution of the molecular minor axis in the XZ plane. The angle of rotation around the alignment axis is denoted by  $\theta$ , see Fig. 2a. At time  $t = 0$ , a short phase-locked OTC pulse is applied to the ensemble. The electric field is given by

$$\mathcal{E} = \mathcal{E}_1(t) \cos(\omega t) \mathbf{e}_Y + \mathcal{E}_2(t) \cos(2\omega t + \phi_L) \mathbf{e}_Z, \quad (1)$$

where  $\mathbf{e}_{Y,Z}$  are the units vectors along the corresponding laboratory axes,  $\mathcal{E}_i(t)$  are fields' envelopes,  $\omega$  is the carrier frequency of the FW field and  $\phi_L$  is the relative phase between the FW and SH fields. The potential,  $U$  describing the interaction of the laser field with the molecules (to third order in the electric field) is given by<sup>42,43</sup>

$$U = -\frac{1}{2} \alpha_{ij} E_i E_j - \frac{1}{6} \beta_{ijk} E_i E_j E_k, \quad (2)$$

where  $\alpha_{ij}$  are the components of the polarizability tensor,  $\beta_{ijk}$  are the hyperpolarizability tensor components, and  $E_i$  are the components of the electric field. The tensors  $\alpha_{ij}$  and  $\beta_{ijk}$  are symmetric in all indices<sup>42</sup> and summation over the repeated indices is implied. For molecules having  $C_{2v}$  symmetry the hyperpolarizability tensor has three independent elements  $\beta_{113}$ ,  $\beta_{223}$  and  $\beta_{333}$ . For SO<sub>2</sub> molecule, index 1 corresponds to the major O-axis, 3 to the minor S-axis and 2 to third principal axis that points out of the molecular plane<sup>42,43</sup>.

Explicit expression for the interaction energy averaged over fast optical oscillations as a function of the angle  $\theta$  is given by:

$$U(\theta) = -\mathcal{E}_{20}^2 a \cos(2\theta) + \mathcal{E}_{10}^2 \mathcal{E}_{20} b \cos(\theta), \quad (3)$$

where  $a = (\alpha_{33} - \alpha_{22})/8$ ,  $b = \beta_{113} \cos(\phi_L)/8$  and  $\mathcal{E}_{i0}$  are the amplitudes of the fields. For SO<sub>2</sub> molecules,  $\alpha_{22} < \alpha_{33}$ , and  $\beta_{113} > 0$ . The  $\cos(2\theta)$  term arises from the field interaction with the linear molecular polarizability, while the  $\cos(\theta)$  term results from the hyperpolarizability interaction. Figure 2b shows  $U(\theta)$  for various  $\phi_L$  values. As seen, the potential is a tilted double well with the tilt controlled by the relative phase  $\phi_L$ . When the relative phase is  $\phi_L = \pi/2$ , then  $b = 0$  and the graph of

the potential is the solid-green curve (Fig. 2b). In this case, the potential is a symmetric function of  $\theta$  in the interval  $[0, \pi]$  and its two minima are equivalent. A kick by such a potential leads the focusing of the angular distribution at  $\theta = 0, \pi$  shortly after the kick.<sup>23</sup> If  $\phi_L \neq \pi/2$ , the symmetry of the potential function is broken and the minima are no longer equivalent, manifested in asymmetrical evolution of the angular distribution. Near the minima ( $\theta = 0, \pi$ ), the potential may be approximated as

$$U(\theta) \approx \begin{cases} (-A + B) + \kappa_- \theta^2 & \theta \approx 0 \\ (-A - B) + \kappa_+ (\theta - \pi)^2 & \theta \approx \pi \end{cases}, \quad (4)$$

where  $A = \mathcal{E}_{20}^2 a$ ,  $B = \mathcal{E}_{10}^2 \mathcal{E}_{20} b$  and  $\kappa_{\mp} = [4A \mp B]/2$ .

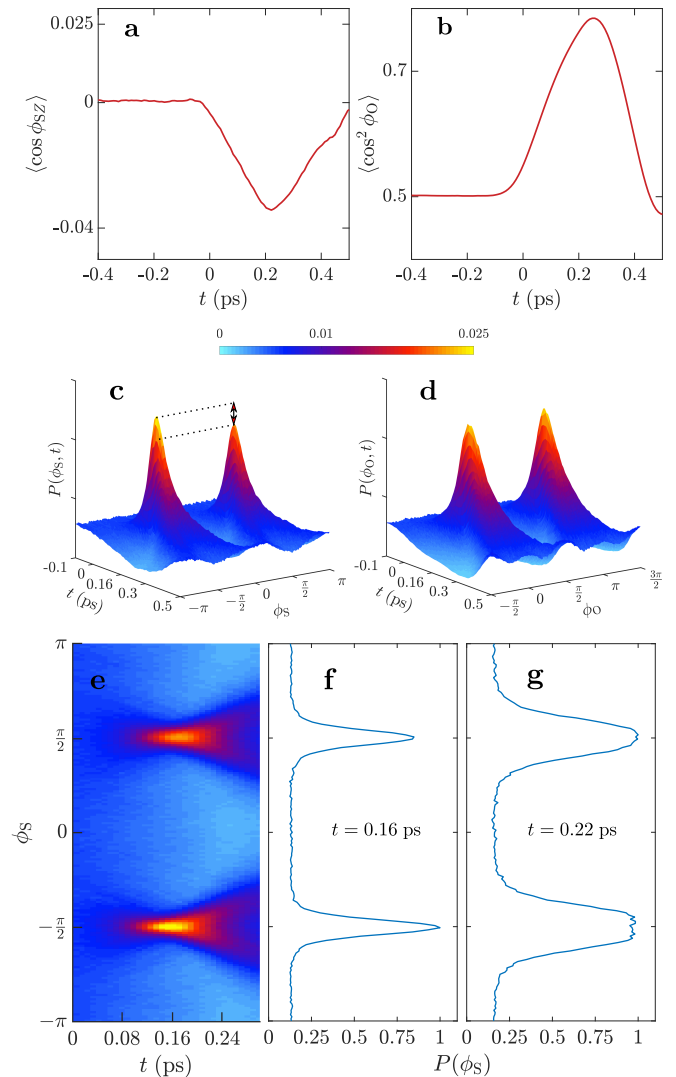


FIG. 3. **Results of 3D simulation.** **a**, Orientation factor  $\langle \cos \phi_{SZ} \rangle(t)$  **b**, Alignment factor  $\langle \cos^2 \phi_O \rangle(t)$ . **c**, 3D surface plot of the time dependent angular distribution for S-axis. **d**, 3D surface plot of the time dependent angular distribution for O-axis. **e**, Top view of the 3D surface for S-axis. **f**, Angular distribution,  $P(\phi_S)$  at  $t = 0.16$  ps, the moment of tight focus at  $\phi_S = -\pi/2$ . **g**, Angular distribution of,  $P(\phi_S)$  at  $t = 0.22$  ps, the moment of maximal orientation.

As seen, the functional form of  $U(\theta)$  is an upward opening parabola both at  $\theta = 0$  and  $\theta = \pi$ . However, the depths of these parabolas (relative difference is  $2B$ ), as well as stiffnesses,  $\kappa_{\mp}$  ( $0 < \kappa_-, \kappa_+$ ) differ. In addition, the maximum of the potential shifts either to the left ( $\phi_L < \pi/2$ ), meaning that more molecules are kicked

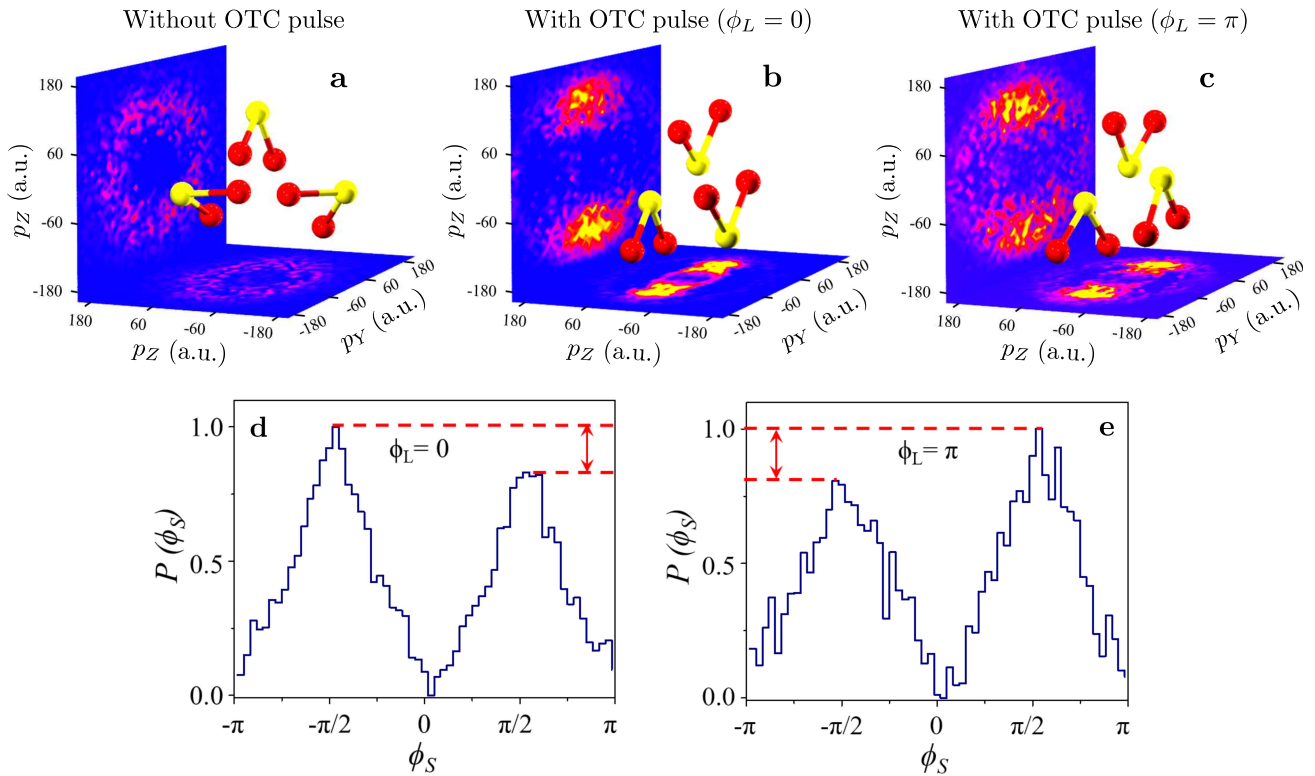


FIG. 4. **Coincidentally measured momentum distributions of  $S^+$  and  $O^+$ .** Here  $p_Y$  and  $p_Z$  are the projections of fragments' momenta on  $Y$  and  $Z$  axes, respectively (measured in atomic units). **a**, Isotropic momentum distribution for  $S^+$  and  $O^+$  ions measured before the arrival of OTC pulse. **b** and **c**, Anisotropic momentum distributions for  $S^+$  and  $O^+$  ions measured at  $t \approx 0.20$  ps after the application of the OTC pulse at  $\phi_L = 0$  and  $\pi$ , respectively. **d** and **e**, Angular distributions of  $S^+$  derived from **b** and **c**, respectively.

towards  $\theta = \pi$ , or to the right ( $\phi_L > \pi/2$ ), in which case more molecules are kicked towards  $\theta = 0$ . Moreover, the focusing times at  $\theta = 0, \pi$  depend on the stiffnesses,  $\kappa_{\mp}$ . For example, in the case of  $\phi_L = 0$  (blue- $\Delta$  curve, Fig. 2b),  $\kappa_- < \kappa_+$  and shortly after the kick, the angular distribution first focuses at  $\theta = \pi$ , and afterwards at  $\theta = 0$ , resulting in a pronounced left-right asymmetry of the angular distribution at the moment of each focusing event. Being an integrated quantity, the orientation factor,  $\langle \cos \theta \rangle(t)$  is almost insensitive to the sharp features of the distribution. It does not attain its maximal value at the moment of the highest left-right asymmetry of the distribution, but rather at the moment when the difference in the areas under the distribution curve to either side of  $\theta = 0$  is the largest. For this reason, in discussions of the simulation and experimental results below we will report both measures of orientation.

The degree of orientation of the S-axis along the Z axis in a molecular ensemble is determined by the balance between aligning and orienting interactions with SH field, as described by the first and the second terms in Eq. 3, respectively. The orientation effect is emphasized relative to the alignment with reduction of SH field amplitude, because the aligning interaction is quadratic in  $\mathcal{E}_{20}$ , while the orienting interaction is linear. Although the optimization of the orientation process is not a subject of the present study, it is worth mentioning that splitting of a two-color pulse into two subpulses may be beneficial for the overall degree of orientation<sup>44</sup>.

As a next step, we proceed to a full three-dimensional simulation of the orientation process. Consider a thermal ( $T = 18$  K) ensemble of  $N \gg 1$  asymmetric classical rigid rotors with known polarizability and hyperpolariz-

ability tensors, which are subject to a phase-locked OTC pulse. To simulate the time-dependent rotational dynamics of the molecules, we adopt an efficient singularity-free numerical technique, where quaternions are used to parametrize the rotation<sup>45–47</sup>. The angular velocity of each molecule is obtained by numerical integration of the Euler equations<sup>48</sup>. The orientation in the laboratory frame of reference is retrieved from numerical integration of the angular-velocity-dependent equation of motion for the quaternion. A detailed description of this computational approach can be found in the Methods Subsection B.

In our Monte Carlo simulations we used ensembles of  $N = 500,000$  molecules that are initially isotropically distributed. To account for the essentially 2D character of the detection setup (Coulomb explosion by a probe pulse circularly polarized in the  $YZ$  plane), and to approximate the experimental measurement conditions, the observable quantities were calculated by averaging over a sub-ensemble of molecules lying approximately in the  $YZ$  plane at the time of the measurement. The selection criterion was based on the angles of both minor and major axes with respect to the  $YZ$  plane. Only when both of them were simultaneously less than  $\pi/4$  (a value close to the experimental arrangement) the molecule was taken into account. The peak intensities of the pulses were  $I_{FW} = 1.4 \times 10^{14}$  W/cm<sup>2</sup> and  $I_{SH} = 0.3 \times 10^{14}$  W/cm<sup>2</sup> and the duration (FWHM) of the pulses was 120 fs, which is much shorter than the typical periods of molecular rotation.

Figures 3a,b plot the simulated orientation of the S-axis (characterized by the  $\langle \cos \phi_{SZ} \rangle$ ) and alignment of the O-axis (characterized by the  $\langle \cos^2 \phi_O \rangle$ ) for various

time delays with respect to the OTC pulse ( $\phi_L = 0$ ). Here  $\phi_O(\phi_{SZ})$  are the angles that the projections of the O-axis(S-axis) on the  $YZ$  plane constitute with respect to the  $Y(Z)$  laboratory axis. For an isotropic molecular ensemble,  $\langle \cos^2 \phi_O \rangle = 0.5$  and  $\langle \cos \phi_{SZ} \rangle = 0.0$ . For the example shown in Fig. 3, both the alignment and the orientation reach maximal values at about 0.22 ps after the excitation by the OTC pulse. Three-dimensional surface plots of the time-dependent probability distributions  $P(\phi_S, t)$  and  $P(\phi_O, t)$  are depicted in Figs. 3c and 3d. Here  $\phi_S$  are the angles that projections of the S-axis on the  $YZ$  plane constitute with respect to the  $Y$  laboratory axis. Figure 3c shows the expected *asymmetric* focusing of the angular distribution of the S-axis at  $\phi_S = -\pi/2, \pi/2$  after 0.16 ps. In analogy to the 2D model considered above, the focusing at  $\phi_S = -\pi/2$  slightly precedes the one at  $\phi_S = \pi/2$  (see Fig. 3e). Moreover, Figure 3f shows a pronounced left-right asymmetry in the distribution of the  $\phi_S$  angle at  $t = 0.16$  ps (ratio of peaks' heights is  $\sim 0.8$ ). The orientation factor attains its maximal value some later ( $t = 0.22$  ps), when the difference of the areas under the distribution curve to either side of  $\phi_S = 0$  is the largest (see Figure 3g). Thus, the effect of orientation is captured by both the asymmetry of the distribution,  $P(\phi_S, t)$  and the integrated quantity,  $\langle \cos \phi_{SZ} \rangle(t)$ . Figure 3d clearly demonstrates the expected symmetric ( $\phi_O = 0, \pi$ ) focusing of angular distribution of the O-axis, which happens simultaneously with the orientation of the S-axis.

Figures 4a-c show the experimentally measured momentum distributions of the coincidentally measured  $S^+$  (vertical plane) and  $O^+$  (horizontal plane) ions ejected from the Coulomb exploded triply ionized  $SO_2$  molecules at 0.20 ps after the application of the OTC pulse. The raw data was normalized to compensate for the detector bias and possible imperfection in the circularity of the probe pulse. The details of the data processing procedure are given in the Methods Subsection A. For the reference, the momentum distribution of the ions ejected from molecules exploded before the application of the OTC pulse (i.e. at negative time delay) is presented in Fig. 4a. In this case, an isotropic angular distribution for both axes is clearly seen. After the application of the OTC pulse, the evident alignment of the major O-axis along the  $Y$  direction (FW polarization) can be seen on the horizontal plane for both laser phases  $\phi_L = 0$  and  $\phi_L = \pi$  (Figs. 4b and 4c). For the minor S-axis, a similar angular clustering along  $Z$  axis, i.e. the direction of the SH polarization, is achieved while exhibiting a noticeable left-right asymmetric distribution. This asymmetry along the  $Z$  axis stands for the laser-induced orientation of the molecular S-axis, which can be controlled by adjusting the laser phase  $\phi_L$  of the OTC pulse. Figures 4d and 4e plot the corresponding angular distributions of the S-axis for the phases of  $\phi_L = 0$  and  $\pi$ , respectively. The orientation degree of the S-axis is estimated to be  $\langle \cos \phi_{SZ} \rangle = -0.069$  for  $\phi_L = 0$  and  $\langle \cos \phi_{SZ} \rangle = 0.043$  for  $\phi_L = \pi$ , respectively. These values are in quantitative agreement with the numerical simulations. The alignment degree of the O-axis is about  $\langle \cos^2 \phi_O \rangle = 0.79$ .

So far, the observed data had been discussed in the traditional terms of the degree of orientation,  $\langle \cos \phi_{SZ} \rangle$ . This is the proper framework when one is dealing with optical experiments, where experimental observation reflect the integrated index of refraction, namely a quantity averaged over all possible molecular orientations. How-

ever, COLTRIMS is different and uniquely offers detailed information on the probability of finding molecules at a specific angle (see Figs. 3c,f for the theoretical results and Figs. 4d,e for the experimental data). As seen in these figures, there is a pronounced difference in the peak values of the distribution for the left  $\phi_S = -\pi/2$  and the right facing molecules  $\phi_S = \pi/2$ . Therefore, we introduce an additional measure of orientation, the differential degree of orientation (DDO), defined as

$$\text{DDO} = \frac{P(\phi_S = \pi/2) - P(\phi_S = -\pi/2)}{P(\phi_S = -\pi/2) + P(\phi_S = \pi/2)}. \quad (5)$$

This measure of orientation is not addressable by the optical detection schemes, but is readily observable in our COLTRIMS experiments. The DDO value obtained from the simulation results is 0.10, while the experimentally measured ones are  $\text{DDO}_{\phi_L=0} = -0.09$  and  $\text{DDO}_{\phi_L=\pi} = 0.11$ . This indicates the ability of the OTC pulse to induce relatively high degree of asymmetry in the otherwise uniform angular distribution of the  $\phi_S$  angle.

In summary, while various different combinations of single and multiple ultrashort pulse excitation were shown to cause molecular alignment, in order to achieve molecular orientation, symmetry breaking must be induced. We have demonstrated, experimentally and theoretically, that field-free three-dimensional molecular orientation can be achieved by phase-locked OTC laser pulse. The relative phase between the two-color fields determines the direction of the oriented molecules in space. The degree of orientation can be controlled by optimizing the parameters (peak intensity and pulse duration) of the laser fields at the fundamental and second harmonic frequencies. For a given total available laser pulse energy, optimal allocation of energy to each component, and/or splitting an OTC pulse in several subpulses may further increase the degree of orientation. To the best of our knowledge, our work provides the first demonstration of field-free, all optical three-dimensional orientation of asymmetric-top molecules. Our approach may find use in the eventual orientation of larger molecules as a step towards their structural analysis by attosecond imaging methodologies<sup>15</sup>.

## REFERENCES

- <sup>1</sup>R. Velotta, N. Hay, M. B. Mason, M. Castillejo, and J. P. Marangos. High-order harmonic generation in aligned molecules. *Phys. Rev. Lett.*, 87:183901, Oct 2001.
- <sup>2</sup>J. Itatani, D. Zeidler, J. Levesque, Michael Spanner, D. M. Villeneuve, and P. B. Corkum. Controlling high harmonic generation with molecular wave packets. *Phys. Rev. Lett.*, 94:123902, Mar 2005.
- <sup>3</sup>Serguei Patchkovskii, Zengxiu Zhao, Thomas Brabec, and D. M. Villeneuve. High harmonic generation and molecular orbital tomography in multielectron systems. *The Journal of Chemical Physics*, 126(11):114306, 2007.
- <sup>4</sup>Manfred Lein. Molecular imaging using recolliding electrons. *Journal of Physics B: Atomic, Molecular and Optical Physics*, 40(16):R135, 2007.
- <sup>5</sup>Jakob Juul Larsen, Ida Wendt-Larsen, and Henrik Stapelfeldt. Controlling the branching ratio of photodissociation using aligned molecules. *Phys. Rev. Lett.*, 83:1123–1126, Aug 1999.
- <sup>6</sup>Masaaki Tsubouchi, Benjamin J. Whitaker, Li Wang, Hiroshi Kohguchi, and Toshinori Suzuki. Photoelectron imaging on time-dependent molecular alignment created by a femtosecond laser pulse. *Phys. Rev. Lett.*, 86:4500–4503, May 2001.



- <sup>7</sup>I. V. Litvinyuk, Kevin F. Lee, P. W. Dooley, D. M. Rayner, D. M. Villeneuve, and P. B. Corkum. Alignment-dependent strong field ionization of molecules. *Phys. Rev. Lett.*, 90:233003, Jun 2003.
- <sup>8</sup>Jochen Küpper, Stephan Stern, Lotte Holmegaard, Frank Filsinger, Arnaud Rouzée, Artem Rudenko, Per Johnsson, Andrew V. Martin, Marcus Adolph, Andrew Aquila, Saša Bajt, Anton Barty, Christoph Bostedt, John Bozek, Carl Caleman, Ryan Coffee, Nicola Coppola, Tjark Delmas, Sascha Epp, Benjamin Erk, Lutz Foucar, Tais Gorkhover, Lars Gumprecht, Andreas Hartmann, Robert Hartmann, Günter Hauser, Peter Holl, Andre Hömke, Nils Kimmel, Faton Krasniqi, Kai-Uwe Kühnel, Jochen Maurer, Marc Messerschmidt, Robert Moshhammer, Christian Reich, Benedikt Rudek, Robin Santra, Ilme Schlichting, Carlo Schmidt, Sebastian Schorb, Joachim Schulz, Heike Soltau, John C. H. Spence, Dmitri Starodub, Lothar Strüder, Jan Thøgersen, Marc J. J. Vrakking, Georg Weidenspointner, Thomas A. White, Cornelia Wunderer, Gerard Meijer, Joachim Ullrich, Henrik Stapelfeldt, Daniel Rolles, and Henry N. Chapman. X-ray diffraction from isolated and strongly aligned gas-phase molecules with a free-electron laser. *Phys. Rev. Lett.*, 112:083002, Feb 2014.
- <sup>9</sup>J. M. Glowina, A. Natan, J. P. Cryan, R. Hartsock, M. Kozina, M. P. Minitti, S. Nelson, J. Robinson, T. Sato, T. van Driel, G. Welch, C. Weninger, D. Zhu, and P. H. Bucksbaum. Self-referenced coherent diffraction x-ray movie of ångström- and femtosecond-scale atomic motion. *Phys. Rev. Lett.*, 117:153003, Oct 2016.
- <sup>10</sup>Jie Yang, Markus Guehr, Xiaozhe Shen, Renkai Li, Theodore Vecchione, Ryan Coffee, Jeff Corbett, Alan Fry, Nick Hartmann, Carsten Hast, Kareem Hegazy, Keith Jobe, Igor Makasyuk, Joseph Robinson, Matthew S. Robinson, Sharon Vetter, Stephen Weathersby, Charles Yoneda, Xijie Wang, and Martin Centurion. Diffractive imaging of coherent nuclear motion in isolated molecules. *Phys. Rev. Lett.*, 117:153002, Oct 2016.
- <sup>11</sup>H. Stapelfeldt and T. Seideman. Colloquium. *Rev. Mod. Phys.*, 75:543–557, Apr 2003.
- <sup>12</sup>Y. Ohshima and H. Hasegawa. Coherent rotational excitation by intense nonresonant laser fields. *International Reviews in Physical Chemistry*, 29(4):619–663, 2010.
- <sup>13</sup>S. Fleischer, Y. Khodorkovsky, E. Gershnel, Y. Prior, and I. Sh. Averbukh. Molecular alignment induced by ultrashort laser pulses and its impact on molecular motion. *Israel Journal of Chemistry*, 52(5):414–437, 2012.
- <sup>14</sup>M. Lemesko, R. V. Krems, J. M. Doyle, and S. Kais. Manipulation of molecules with electromagnetic fields. *Molecular Physics*, 111(12-13):1648–1682, 2013.
- <sup>15</sup>Junliang Xu, Cosmin I Blaga, Pierre Agostini, and Louis F DiMauro. Time-resolved molecular imaging. *Journal of Physics B: Atomic, Molecular and Optical Physics*, 49(11):112001, 2016.
- <sup>16</sup>Bretislav Friedrich and Dudley Herschbach. Enhanced orientation of polar molecules by combined electrostatic and nonresonant induced dipole forces. *The Journal of Chemical Physics*, 111(14):6157–6160, 1999.
- <sup>17</sup>Hirofumi Sakai, Shinichirou Minemoto, Hiroshi Nanjo, Haruka Tanji, and Takayuki Suzuki. Controlling the orientation of polar molecules with combined electrostatic and pulsed, nonresonant laser fields. *Phys. Rev. Lett.*, 90:083001, Feb 2003.
- <sup>18</sup>Omar Ghafur, Arnaud Rouzée, Arjan Gijsbertsen, Wing Kiu Siu, Steven Stolte, and Marc J. J. Vrakking. Impulsive orientation and alignment of quantum-state-selected molecules. *Nat Phys*, 5(4):289–293, April 2009.
- <sup>19</sup>Lotte Holmegaard, Jens H. Nielsen, Iftach Nevo, Henrik Stapelfeldt, Frank Filsinger, Jochen Küpper, and Gerard Meijer. Laser-induced alignment and orientation of quantum-state-selected large molecules. *Phys. Rev. Lett.*, 102:023001, Jan 2009.
- <sup>20</sup>Akihisa Goban, Shinichirou Minemoto, and Hirofumi Sakai. Laser-field-free molecular orientation. *Phys. Rev. Lett.*, 101:013001, Jun 2008.
- <sup>21</sup>H. Harde, Søren Keiding, and D. Grischkowsky. Thz commensurate echoes: Periodic rephasing of molecular transitions in free-induction decay. *Phys. Rev. Lett.*, 66:1834–1837, Apr 1991.
- <sup>22</sup>C.M. Dion, A.D. Bandrauk, O. Atabek, A. Keller, H. Umeda, and Y. Fujimura. Two-frequency laser orientation of polar molecules. numerical simulations for HCN. *Chemical Physics Letters*, 302(3-4):215–223, 1999.
- <sup>23</sup>I. Sh. Averbukh and R. Arvieu. Angular focusing, squeezing, and rainbow formation in a strongly driven quantum rotor. *Phys. Rev. Lett.*, 87:163601, Sep 2001.
- <sup>24</sup>Mette Machholm and Niels E. Henriksen. Field-free orientation of molecules. *Phys. Rev. Lett.*, 87:193001, Oct 2001.
- <sup>25</sup>Sharly Fleischer, Yan Zhou, Robert W. Field, and Keith A. Nelson. Molecular orientation and alignment by intense single-cycle thz pulses. *Phys. Rev. Lett.*, 107:163603, Oct 2011.
- <sup>26</sup>Kenta Kitano, Nobuhisa Ishii, Natsuki Kanda, Yoshiyuki Matsumoto, Teruto Kanai, Makoto Kuwata-Gonokami, and Jiro Itatani. Orientation of jet-cooled polar molecules with an intense single-cycle thz pulse. *Phys. Rev. A*, 88:061405, Dec 2013.
- <sup>27</sup>D. Daems, S. Guérin, D. Sugny, and H. R. Jauslin. Efficient and long-lived field-free orientation of molecules by a single hybrid short pulse. *Phys. Rev. Lett.*, 94:153003, Apr 2005.
- <sup>28</sup>E. Gershnel, I. Sh. Averbukh, and Robert J. Gordon. Orientation of molecules via laser-induced antialignment. *Phys. Rev. A*, 73:061401, Jun 2006.
- <sup>29</sup>K. N. Egodapitiya, Sha Li, and R. R. Jones. Terahertz-induced field-free orientation of rotationally excited molecules. *Phys. Rev. Lett.*, 112:103002, Mar 2014.
- <sup>30</sup>Ran Damari, Shimshon Kallush, and Sharly Fleischer. Rotational control of asymmetric molecules: Dipole- versus polarizability-driven rotational dynamics. *Phys. Rev. Lett.*, 117:103001, Sep 2016.
- <sup>31</sup>E. Gershnel and I. Sh. Averbukh. Orienting asymmetric molecules by laser fields with twisted polarization. *Phys. Rev. Lett.*, 120:083204, Feb 2018.
- <sup>32</sup>A. Yachmenev and S. N. Yurchenko. Detecting chirality in molecules by linearly polarized laser fields. *Phys. Rev. Lett.*, 117:033001, Jul 2016.
- <sup>33</sup>Ilya Tutunnikov, Erez Gershnel, Shachar Gold, and Ilya Sh. Averbukh. Selective orientation of chiral molecules by laser fields with twisted polarization. *The Journal of Physical Chemistry Letters*, 9(5):1105–1111, 2018. PMID: 29417812.
- <sup>34</sup>Marc J.J. Vrakking and Steven Stolte. Coherent control of molecular orientation. *Chemical Physics Letters*, 271(4-6):209–215, 1997.
- <sup>35</sup>Tsuneto Kanai and Hirofumi Sakai. Numerical simulations of molecular orientation using strong, nonresonant, two-color laser fields. *The Journal of Chemical Physics*, 115(12):5492–5497, 2001.
- <sup>36</sup>S. De, I. Znakovskaya, D. Ray, F. Anis, Nora G. Johnson, I. A. Bocharova, M. Magrakvelidze, B. D. Esry, C. L. Coker, I. V. Litvinyuk, and M. F. Kling. Field-free orientation of molecules by femtosecond two-color laser fields. *Phys. Rev. Lett.*, 103:153002, Oct 2009.
- <sup>37</sup>Keita Oda, Masafumi Hita, Shinichirou Minemoto, and Hirofumi Sakai. All-optical molecular orientation. *Phys. Rev. Lett.*, 104:213901, May 2010.
- <sup>38</sup>Jian Wu and Heping Zeng. Field-free molecular orientation control by two ultrashort dual-color laser pulses. *Phys. Rev. A*, 81:053401, May 2010.
- <sup>39</sup>E. Frumker, C. T. Hebeisen, N. Kajumba, J. B. Bertrand, H. J. Wörner, M. Spanner, D. M. Villeneuve, A. Naumov, and P. B. Corkum. Oriented rotational wave-packet dynamics studies via high harmonic generation. *Phys. Rev. Lett.*, 109:113901, Sep 2012.
- <sup>40</sup>Norio Takemoto and Kaoru Yamanouchi. Fixing chiral molecules in space by intense two-color phase-locked laser fields. *Chemical Physics Letters*, 451(1):1–7, 2008.
- <sup>41</sup>R. Dörner, V. Mergel, O. Jagutzki, L. Spielberger, J. Ullrich, R. Moshhammer, and H. Schmidt-Böcking. Cold target recoil ion momentum spectroscopy: a momentum microscope to view atomic collision dynamics. *Physics Reports*, 330(2):95–192, 2000.
- <sup>42</sup>A. D. Buckingham and B. J. Orr. Molecular hyperpolarizabilities. *Q. Rev. Chem. Soc.*, 21:195–212, 1967.
- <sup>43</sup>George Maroulis. The electric hyperpolarizability of ozone and sulfur dioxide. *Chemical Physics Letters*, 189(2):112–118, 1992.
- <sup>44</sup>Shian Zhang, Chenhui Lu, Tianqing Jia, Zugeng Wang, and Zhenrong Sun. Field-free molecular orientation enhanced by two dual-color laser subpulses. *The Journal of Chemical Physics*, 135:034301, 2011.
- <sup>45</sup>D. C. Rapaport. *The Art of Molecular Dynamics Simulation*. Cambridge University Press, 2 edition, 2004.
- <sup>46</sup>L. Romero E. A. Coutias. The quaternions with an application to rigid body dynamics. Techreport, University of New Mexico, Albuquerque, NM 87131, Feb 1999.
- <sup>47</sup>J. B. Kuipers. *Quaternions and Rotation Sequences: A Primer with Applications to Orbits, Aerospace and Virtual Reality*. Princeton University Press, 2002.
- <sup>48</sup>L.D. Landau and E.M. Lifshitz. *Mechanics*. Butterworth-Heinemann, Oxford, Third edition, 1976.

## ACKNOWLEDGMENTS

This work is supported by the National Natural Science Foundation of China (Grant Nos. 11425416, 61690224 and 11761141004), the 111 Project of China (Grant No. B12024), the Israel Science Foundation (Grant No. 746/15), the ICORE program “Circle of Light”, and the ISF-NSFC (Grant No. 2520/17). I.A. acknowledges support as the Patricia Elman Bildner Professorial Chair. This research was made possible in part by the historic generosity of the Harold Perlman Family.

## AUTHOR CONTRIBUTIONS

K.L. and I. T. contributed equally to this work. K.L., J.Q., J.M., Q.S., Q.J., W.Z., H.L., F.S., X.G., H.L., P.L., H.Z. and J.W. designed and performed the experiments, I.T. and I.A. carried out the theoretical analysis and numerical simulations. Y.P., I.A. and J.W. jointly supervised the whole project. K.L., I.T., Y.P., I.A., and J.W. wrote the manuscript. All authors contributed to the analyses and discussions of the results.

## COMPETING FINANCIAL INTERESTS

The authors declare no competing financial interests.

## METHODS

### A. Experimental Methods

Field-free 3D orientation of  $\text{SO}_2$  molecule in a molecular beam is induced by a pair of orthogonally polarized two-color femtosecond laser pulses. Following the orientation, an intense circularly polarized probe pulse Coulomb-explodes the molecules to image their spatial orientation at various time delays, as schematically shown in Fig. 1. The output (25 fs, 790 nm, 10 kHz) of a Femtolasers multipass amplifier Ti:sapphire laser system is split into pump and probe arms via a beam splitter of 7 : 3 intensity ratio. The OTC pulse is generated in a collinear scheme by down-collimating the 70% pump beam into a 150  $\mu\text{m}$ -thick  $\beta$ -barium borate ( $\beta$ -BBO) crystal to generate a SH pulse at 395 nm. To increase the doubling efficiency, a telescope is placed in front of the  $\beta$ -BBO crystal to reduce the beam diameter by a factor of two. A path of 7 mm-thick  $\alpha$ -barium borate ( $\alpha$ -BBO) crystals is introduced after the  $\beta$ -BBO crystal to compensate the group delay between the two colors that is induced by the optical components (wedges, mirrors and windows) along the beams’ path. The 30% probe beam is passed through a quarter wave plate, followed by a beam expander, making it circularly polarized and doubles its diameter. A motorized delay stage in the probe arm is used to synchronize and adjust its time delay with respect to the OTC pulse. The two pulses are afterwards focused onto a supersonic molecular beam of 20% mixture of  $\text{SO}_2$  in He in an ultrahigh vacuum chamber of

the COLTRIMS apparatus by a concave silver mirror ( $f = 7.5$  cm).

By pre-compensation the pulse chirp prior to the amplifier, the temporal duration of the probe pulse in the interaction region is controlled to be  $\sim 40$  fs. The OTC pulse is stretched to be  $\sim 120$  fs after the BBO crystals, wedge pair, the combination mirror and the entrance window. The intensities of the FW and the SH in the reaction area are measured to be  $I_{\text{FH}} \approx 1.4 \times 10^{14}$  W/cm<sup>2</sup>,  $I_{\text{SH}} \approx 0.3 \times 10^{14}$  W/cm<sup>2</sup> and the intensity of the probe pulse is  $\sim 6 \times 10^{14}$  W/cm<sup>2</sup>. The rotational temperature of the molecular beam is close to the translation temperature, which can be estimated from  $T_{\text{trans}} = \Delta p^2 / [4 \ln(4) k_B m]$ , where  $k_B$  is the Boltzmann’s constant,  $\Delta p$  and  $m$  are the full-width at half-maximum of the momentum distribution (in the jet direction) and mass of the singly ionized  $\text{SO}_2^+$ , respectively. In our experiment we measure a momentum width in the jet direction of  $\Delta p \sim 6.1$  a.u. of  $\text{SO}_2^+$  ions created by a laser field polarized along the  $Z$  axis (orthogonal to the jet direction). The rotational temperature of the  $\text{SO}_2$  molecule is estimated to be 18 K. The produced fragment ions are accelerated and guided by a weak homogeneous static electric field ( $\sim 20$  V/cm) and then detected by a time- and position-sensitive microchannel plate detector. The three-dimensional momenta of the ions are retrieved from the measured time-of-flights and positions of the impacts. Here, for the asymmetric-top molecules, the direction of the principle axes is retrieved from the coincidentally measured fragment ions of the triple-ionization-induced Coulomb explosion channel of  $[\text{SO}_2 + n\hbar\omega \rightarrow \text{S}^+ + \text{O}^+ + \text{O}^+ + 3e]$ . The angular distributions for  $\phi_{\text{S}}$  and  $\phi_{\text{O}}$  away from the  $Y$  axis at maximum 3D orientation are measured by fixing the delay stage around 0.20 ps. To increase the visibility and eliminate the bias induced by the imperfect circularity of the probe pulse, the angular distribution at negative time delay is collected as reference for the data analysis. We normalize the total probability of the angular distribution to unity for each time delay and then subtract the averaged angular distribution at negative times. Since the fragmentation of triply ionized  $\text{SO}_2$  molecule happens mostly in the polarization plane of the probe pulse, the data analysis are restricted to this plane by selecting molecules confined to  $[-\pi/4, \pi/4]$  with respect to the  $YZ$  plane.

### B. Numerical Methods

We consider the asymmetric molecules as classical rigid rotors with anisotropic polarizability and hyperpolarizability. A specific example of the  $\text{SO}_2$  molecule is presented in Figure 5.

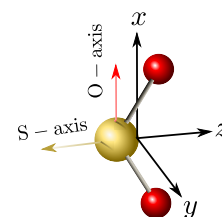


FIG. 5. The  $\text{SO}_2$  molecule. Axes  $x$ ,  $y$  and  $z$  are the principal axes of the molecule. Here, all atoms lie in  $xz$  plane and color-coded: red - oxygen, yellow - sulfur.

Table I summarizes the properties of the SO<sub>2</sub> molecule. The moment of inertia tensor and its principal axes were computed based on the Cartesian atomic coordinates (measured in bohr)<sup>43</sup>: S = (0.0, 0.0, -0.682958) and O = (±2.333567, 0.0, 0.682581).

| $\overset{\leftrightarrow}{\mathbf{I}}$ comp. | $\overset{\leftrightarrow}{\boldsymbol{\alpha}}$ comp. | $\overset{\leftrightarrow}{\boldsymbol{\beta}}$ com. | $\mathbf{D}$ comp. |
|---|--|--|--------------------|
| $I_x = 55509$                                 | $\alpha_{xx} = 31.26$                                  | $\beta_{xxz} = 22.0$                                 | $\mu_x = 0.0$      |
| $I_y = 371885$                                | $\alpha_{yy} = 18.64$                                  | $\beta_{yyz} = 26.5$                                 | $\mu_y = 0.0$      |
| $I_z = 317477$                                | $\alpha_{zz} = 20.80$                                  | $\beta_{zzz} = 6.4$                                  | $\mu_z = -0.79$    |

TABLE I. Summary of the SO<sub>2</sub> properties (measured in a.u): eigenvalues of the moment of inertia tensor, components of polarizability tensor, components of hyperpolarizability tensor and components of dipole moment in the body-fixed frame of molecular principal axes.

We investigate the behavior of an ensemble of  $N \gg 1$  molecules with the help of the Monte Carlo simulation in which rotational dynamics of each molecule is treated numerically. The description of rotational dynamics in terms of Euler angles is known to lead to singular equations of motion<sup>48</sup>. Here, we rely on an efficient singularity-free numerical technique where quaternions are used to parametrize the rotation<sup>45-47</sup>. This approach solves the singularity problem and avoids time consuming calculations of trigonometric functions. The orientation of a rigid body is described by a quaternion:

$$q = (q_0, q_1, q_2, q_3) = \left( \cos \frac{\theta}{2}, \sin \frac{\theta}{2} \mathbf{p} \right),$$

where  $\mathbf{p}$  is a unit vector defining the direction of rotation and  $\theta$  is the angle of rotation about it. The rate of change in time of a quaternion is given by

$$\dot{q} = \frac{1}{2} q \Omega, \quad (6)$$

where  $\Omega = (0, \boldsymbol{\Omega})$  is a pure quaternion<sup>46,47</sup> constructed from angular velocity of the molecule, expressed with respect to the body-fixed frame of molecular principal axes  $a$ ,  $b$  and  $c$ ,  $\boldsymbol{\Omega} = (\Omega_a, \Omega_b, \Omega_c)$ . In Eq. 6, the quaternions multiplication rule is implied<sup>46,47</sup>. According to Euler equation<sup>48</sup>, the rate of change of the angular velocity expressed with respect to the body-fixed frame is

$$\overset{\leftrightarrow}{\mathbf{I}} \dot{\boldsymbol{\Omega}} = \left( \overset{\leftrightarrow}{\mathbf{I}} \boldsymbol{\Omega} \right) \times \boldsymbol{\Omega} + \mathbf{T}, \quad (7)$$

where  $\overset{\leftrightarrow}{\mathbf{I}}$  is the moment of inertia tensor and  $\mathbf{T} = (T_a, T_b, T_c)$  is the torque, both expressed with respect

to the body-fixed frame. To model the torque due to interaction with an electric field, we transform the electric field  $\boldsymbol{\mathcal{E}}$ , expressed with respect to the laboratory frame of reference, into the body-fixed frame. The transformation rule is  $E = q^c \boldsymbol{\mathcal{E}} q$ , where  $E = (0, \mathbf{E})$  and  $\boldsymbol{\mathcal{E}} = (0, \boldsymbol{\mathcal{E}})$  are pure quaternions, constructed from the electric field in the body-fixed frame and  $\boldsymbol{\mathcal{E}}$ , respectively. A conjugate of a quaternion  $q$  is denoted by  $q^c$ .<sup>46,47</sup> Again, quaternions multiplication rule is used in the transformation. The linear polarizability part of the induced dipole moment in the body-fixed principal axes frame is given by  $\mathbf{D} = \overset{\leftrightarrow}{\boldsymbol{\alpha}} \mathbf{E}$ , where  $\overset{\leftrightarrow}{\boldsymbol{\alpha}}$  is the polarizability tensor in the body-fixed frame. The torque due to the polarizability is  $\mathbf{T}^\alpha = \langle \mathbf{D} \times \mathbf{E} \rangle$ , where  $\langle \cdot \rangle$  is a time average over fast oscillations of the optical field. The torque due to the hyperpolarizability in the body fixed frame is given by  $\mathbf{T}_i^\beta = \langle \varepsilon_{ijk} \beta_{jnm} E_n E_m E_k \rangle$ , where  $\varepsilon_{ijk}$  is the Levi-Civita symbol. Explicit torques expressions for the two-color field are

$$\mathbf{T}^\alpha = \frac{\mathcal{E}_1^2}{2} \left( \overset{\leftrightarrow}{\boldsymbol{\alpha}} \mathbf{E}_1 \right) \times \mathbf{E}_1 + \frac{\mathcal{E}_2^2}{2} \left( \overset{\leftrightarrow}{\boldsymbol{\alpha}} \mathbf{E}_2 \right) \times \mathbf{E}_2$$

and

$$T_i^\beta = \frac{\mathcal{E}_1^2 \mathcal{E}_2}{4} \varepsilon_{ijk} \left[ \beta_{mnj} E_{1m} E_{2n} E_{1k} + \frac{1}{2} \beta_{mnj} E_{1m} E_{1n} E_{2k} \right],$$

where  $\mathbf{E}_1$ ,  $\mathbf{E}_2$  are the transformed (into the body-fixed frame) polarization vectors of the FW and SH, respectively.

In our simulations, the initial ensemble of molecules is generated via a Monte Carlo procedure. The initial orientations of the molecules and the corresponding quaternions for an isotropic ensemble are generated by a random uniform sampling over the space of rotations<sup>49</sup>. We assume that the molecular ensemble is initially at thermal conditions, and that the molecular angular velocities are distributed according to:

$$f(\boldsymbol{\Omega}) \propto \exp \left[ -\frac{\boldsymbol{\Omega}^T \overset{\leftrightarrow}{\mathbf{I}} \boldsymbol{\Omega}}{2k_B T} \right] = \prod_i \exp \left[ -\frac{I_i \Omega_i^2}{2k_B T} \right],$$

where  $i = x, y, z$ . Since the kinetic energy is a scalar, it is coordinate invariant so we express it with respect to the body-fixed frame. Here,  $T$  is the temperature of the gas and  $k_B$  is the Boltzmann constant. We integrate the system of equations 6 and 7 using the Runge-Kutta integration method. At each time step, the quaternions are renormalized in order to preserve the unit norm<sup>45,47</sup>.